PNAS RESEARCH ARTICLE | EARTH, ATMOSPHERIC, AND PLANETARY SCIENCES

Tripling of western US particulate pollution from wildfires in a warming climate

Yuanyu Xie[a,b,1], Meiyun Lin[a,b,1], Bertrand Decharme[c], Christine Delire[c], Larry W. Horowitz[b], David M. Lawrence[d], Fang Li[e], and Roland Séférian[c]

Edited by Akkihebbal Ravishankara, Colorado State University, Fort Collins, CO; received June 22, 2021; accepted February 11, 2022

The air quality impact of increased wildfires in a warming climate has often been overlooked in current model projections, owing to the lack of interactive fire emissions of gases and particles responding to climate change in Earth System Model (ESM) projection simulations. Here, we combine multiensemble projections of wildfires in three ESMs from the Sixth Coupled Model Intercomparison Project (CMIP6) with an empirical statistical model to predict fine particulate ($PM_{2.5}$) pollution in the late 21st century under a suite of Shared Socioeconomic Pathways (SSPs). Total CO_2 emissions from fires over western North America during August through September are projected to increase from present-day values by 60 to 110% (model spread) under a strong-mitigation scenario (SSP1-2.6), 100 to 150% under a moderate-mitigation scenario (SSP2-4.5), and 130 to 260% under a low-mitigation scenario (SSP5-8.5) in 2080–2100. We find that enhanced wildfire activity under SSP2-4.5 and SSP5-8.5 could cause a twofold to threefold increase in $PM_{2.5}$ pollution over the US Pacific Northwest during August through September. Even with strong mitigation under SSP1-2.6, $PM_{2.5}$ in the western US would increase ∼50% by midcentury. By 2080–2100, under SSP5-8.5, the 95th percentile of late-summer daily $PM_{2.5}$ may frequently reach unhealthy levels of 55 to 150 μg/m^3. In contrast, chemistry-climate models using prescribed fire emissions of particles not responding to climate change simulate only a 7% increase in $PM_{2.5}$. The consequential pollution events caused by large fires during 2017–2020 might become a new norm by the late 21st century, with a return period of every 3 to 5 y under SSP5-8.5 and SSP2-4.5.

air quality | fires | drought | climate warming | Earth System Models

Significance

Record-setting fires in the western United States over the last decade caused severe air pollution, loss of human life, and property damage. Enhanced drought and increased biomass in a warmer climate may fuel larger and more frequent wildfires in the coming decades. Applying an empirical statistical model to fires projected by Earth System Models including climate–ecosystem–socioeconomic interactions, we show that fine particulate pollution over the US Pacific Northwest could double to triple during late summer to fall by the late 21st century under intermediate- and low-mitigation scenarios. The historic fires and resulting pollution extremes of 2017–2020 could occur every 3 to 5 y under 21st-century climate change, posing challenges for air quality management and threatening public health.

Wildfires contribute 15 to 30% of atmospheric primary fine particulate matter ($PM_{2.5}$) emissions in the United States (1), with implications for ecosystems, human health, and climate (2–5). Marked increases in wildfire-burned area over the western United States in recent decades have been linked to anthropogenic climate change and land management practices (4, 6–8). Increasing emissions from wildfires have caused summertime $PM_{2.5}$ levels to rise in some western US regions, despite efforts to control anthropogenic emissions (9–11). Millions of people were exposed to very unhealthy or hazardous $PM_{2.5}$ concentrations (150 to 650 μg/m^3 for 24-h average) for extended periods during recent large wildfires around the world (11–17). Exposure to dense smoke from fires has detrimental effects on human health (3, 18–20), with an economic cost due to short-term smoke exposure estimated to be $11 billion to $20 billion per year in the continental United States (21). The US Clean Air Act allows for screening of air quality exceedances caused by "exceptional events," such as wildfires, from counting toward a nonattainment determination (22). Understanding the extent to which wildfire emissions in a future climate influence $PM_{2.5}$ exceedances thus has implications for designing effective air quality policies.

A number of studies have projected enhanced wildfire activity over the western United States under a warming climate during the 21st century (23–27). However, owing to the lack of interactive fire emissions of gases and particles responding to climate change in current chemistry-climate models, projections of future $PM_{2.5}$ air quality generally overlook the impacts of changing fires (28–31). A few studies estimated future fire emissions using statistical regressions of burned area and climate variables and fed these emissions into an offline chemical transport model to estimate future $PM_{2.5}$ air quality (26, 32–35). These studies suggested 80 to 170% increases in fire emissions of primary aerosols by the 2050s, which would result in 46 to 70% increases in surface organic carbon concentrations (a key component in fire smoke). Using fire emissions simulated by a process-based fire model driven by archived meteorological fields from a chemistry-climate model, several studies estimated 50 to 90% increases in mean organic carbon concentrations over the continental United States by the late 21st

Author contributions: M.L. designed research; Y.X. and M.L. performed research; B.D., C.D., L.W.H., D.M.L., F.L., and R.S. contributed new reagents/analytic tools; Y.X. analyzed data; Y.X. and M.L. wrote the paper; and B.D., C.D., L.W.H., D.M.L., F.L., and R.S. contributed to discussions and improving the manuscript.

The authors declare no competing interest.

This article is a PNAS Direct Submission.

[1]To whom correspondence may be addressed. Email: Yuanyu.Xie@noaa.gov or Meiyun.Lin@noaa.gov.

This article contains supporting information online at http://www.pnas.org/lookup/suppl/doi:10.1073/pnas.2111372119/-/DCSupplemental.

Published March 28, 2022.

century (23, 36). These results have large uncertainties, as the statistical or offline fire models typically do not include feedbacks among climate, land use, ecosystem dynamics, and anthropogenic influences through ignition and suppression (2, 37–39).

Here, we leverage the Sixth Coupled Model Intercomparison Project (CMIP6) multimodel and multiensemble simulations of fire CO_2 emissions responding to changes in climate, vegetation, and population distributions, combined with a multiple linear regression (MLR) model developed from historical observations, to project wildfire impacts on $PM_{2.5}$ means and extremes over the western United States under a suite of Shared Socioeconomic Pathways (SSPs; *Materials and Methods*). The process-based fire models in CMIP6 are greatly improved compared to those in CMIP5, with better representation of the impacts of fuel wetness on fire occurrence and spread, enhanced fire spread rate in forest crowns, and the ability to simulate multiday fires (40–51). Our statistical model considers the influence of both local and regional fires, as well as interstate smoke transport, air stagnation, and other meteorological conditions. We compare our MLR-predicted $PM_{2.5}$ with that simulated in the chemistry-climate models using prescribed fire emissions of gases and particles not responding to climate change (*Materials and Methods*) (29). We show that drought and increased biomass under a warmer climate increase the risk of fires in the Pacific Northwest during the late 21st century, causing a twofold to threefold increase in $PM_{2.5}$ levels in late summer to fall.

Results

Observed Correlations between Fires and $PM_{2.5}$ Air Quality. We first use historical observations to investigate the extent to which the interannual variability of $PM_{2.5}$ means and extremes at US surface sites can be explained by regional versus local fires, as well as meteorological conditions. The observed relationships will serve as a basis for developing the MLR model used to predict future $PM_{2.5}$ levels from fire CO_2 emissions and meteorology available from CMIP6 Earth System Models. We correlate surface $PM_{2.5}$ observations averaged over a 2° × 2° grid with fire CO_2 emissions integrated over a box with size varying from 2.5° × 2.5° to 20° × 20° centered at that grid during May through November from 1997 to 2020, using simple linear regression and MLR (*Materials and Methods*). We consider four meteorological variables: surface temperature, precipitation, relative humidity, and air stagnation, which have been shown to be correlated with surface $PM_{2.5}$ (11, 52).

During August and September, when fires peak seasonally over the Pacific Northwest under the present-day climate (53), mean $PM_{2.5}$ levels at western US sites show strong correlations (r^2 = 0.5 to 0.9) with regional fire CO_2 emissions summed over a box of 10° × 10° to 15° × 15°, indicating the importance of regional smoke transport (11) (Fig. 1*A*). In comparison, the correlations are much weaker ($r^2 < 0.5$) during May through July and October through November (*SI Appendix*, Fig. S1) and are statistically insignificant ($P > 0.05$) at most eastern US sites, where fire is not the dominant source of surface $PM_{2.5}$. In the following analyses, we thus focus on the US Pacific Northwest (solid black box in Fig. 1*B*) during August and September.

The MLR model, including the impacts from meteorological variables, achieves higher correlations (r^2 = 0.7 to 0.9; Fig. 1*B*) compared to the simple linear regression with fires alone (r^2 = 0.5 to 0.9; Fig. 1*A*). Fire CO_2 emissions on average explain 66% of the observed $PM_{2.5}$ interannual variability during August through September in the Pacific Northwest (Fig. 1*C*), with air stagnation index being the second most important predictor (11%), consistent with our prior work suggesting that air stagnation played an important role in the accumulation of $PM_{2.5}$ during the historic 2017 and 2018 fire seasons (11). The contributions from relative humidity, temperature, and precipitation are each less than 10%. A larger increase in correlation (r^2) with meteorology is found in July and October than in August or September, suggesting a more important role of meteorology in controlling $PM_{2.5}$ during these months (*SI Appendix*, Fig. S1). These correlations confirm that it is important to consider impacts from both fires and meteorology for a robust estimation of changes in future $PM_{2.5}$ air quality.

We next examine the relationship between regional fires and $PM_{2.5}$ extremes, defined as the 95th percentile (q95) of available daily $PM_{2.5}$ measurements from all sites within a 2° × 2° grid for August and September (*Materials and Methods* and *SI Appendix*, Fig. S2). We still use monthly mean meteorological variables, instead of extremes, in the MLR model since the q95 $PM_{2.5}$ in observations may not coincide with days having extreme meteorological conditions (i.e., heat wave or stagnation), and there are larger uncertainties in the predicted climate extremes than mean states. Significant correlations are observed between fire CO_2 emissions and the q95 $PM_{2.5}$ at most western US sites in August and September, based on simple linear regression (r^2 = 0.5 to 0.9; Fig. 1*D*) and MLR (r^2 = 0.7 to 0.9; Fig. 1*E*). Fire CO_2 emissions explain 70% of the observed $PM_{2.5}$ interannual variability, on average, at US Pacific Northwest sites (Fig. 1*F*), dominating over meteorological impacts.

The interannual variability of both mean and q95 $PM_{2.5}$ during August through September averaged over US Pacific Northwest sites shows a strong correlation (r^2 = 0.8 to 0.9) with regional total fire CO_2 emissions over western North America (Fig. 1 *G* and *H*). In the 2017, 2018, and 2020 fire seasons, the western United States experienced record-breaking wildfires burning ∼50% more than the average area over the past two decades (54–56). The q95 $PM_{2.5}$ averaged over the US Pacific Northwest sites during August through September was 76 μg/m^3 in 2017, 44 μg/m^3 in 2018, and 95 μg/m^3 in 2020, respectively, exceeding the US National Ambient Air Quality Standard of 35 μg/m^3.

These MLR analyses demonstrate significant interannual correlations of surface $PM_{2.5}$ pollution with regional fire CO_2 emissions and meteorology over the western United States during August through September. Cross-validation further confirms the robustness of the MLR model in predicting $PM_{2.5}$ (*SI Appendix*, section S1). We obtain regression coefficients for the MLR model using the relationships of $PM_{2.5}$, fires, and meteorological conditions observed in August through September during the period 1997–2020. Then, we drive the MLR model with the monthly time series of fire CO_2 emissions and meteorological variables simulated by CMIP6 Earth System Models under different climate change scenarios to predict $PM_{2.5}$ throughout the 21st century (*Materials and Methods*).

Evaluating Variability of Fires Simulated by CMIP6 Models. To establish the robustness of future projections, we examine how well three CMIP6 models, the Community Earth System Model Version 2 (CESM2) (57), the Geophysical Fluid Dynamics Laboratory Earth System Model Version 4.1 (GFDL-ESM4.1) (58), and the Centre National de Recherches Météorologiques Earth System Model Version 2 (CNRM-ESM2-1) (59), simulate historical fires. We use satellite observations of burned area from the Moderate Resolution Imaging Spectrometer (MODIS) (60) and satellite-based estimates of fire CO_2 emissions from the Global Fire Emissions Database (GFED4s) (61, 62) and the Quick Fire Emissions Dataset

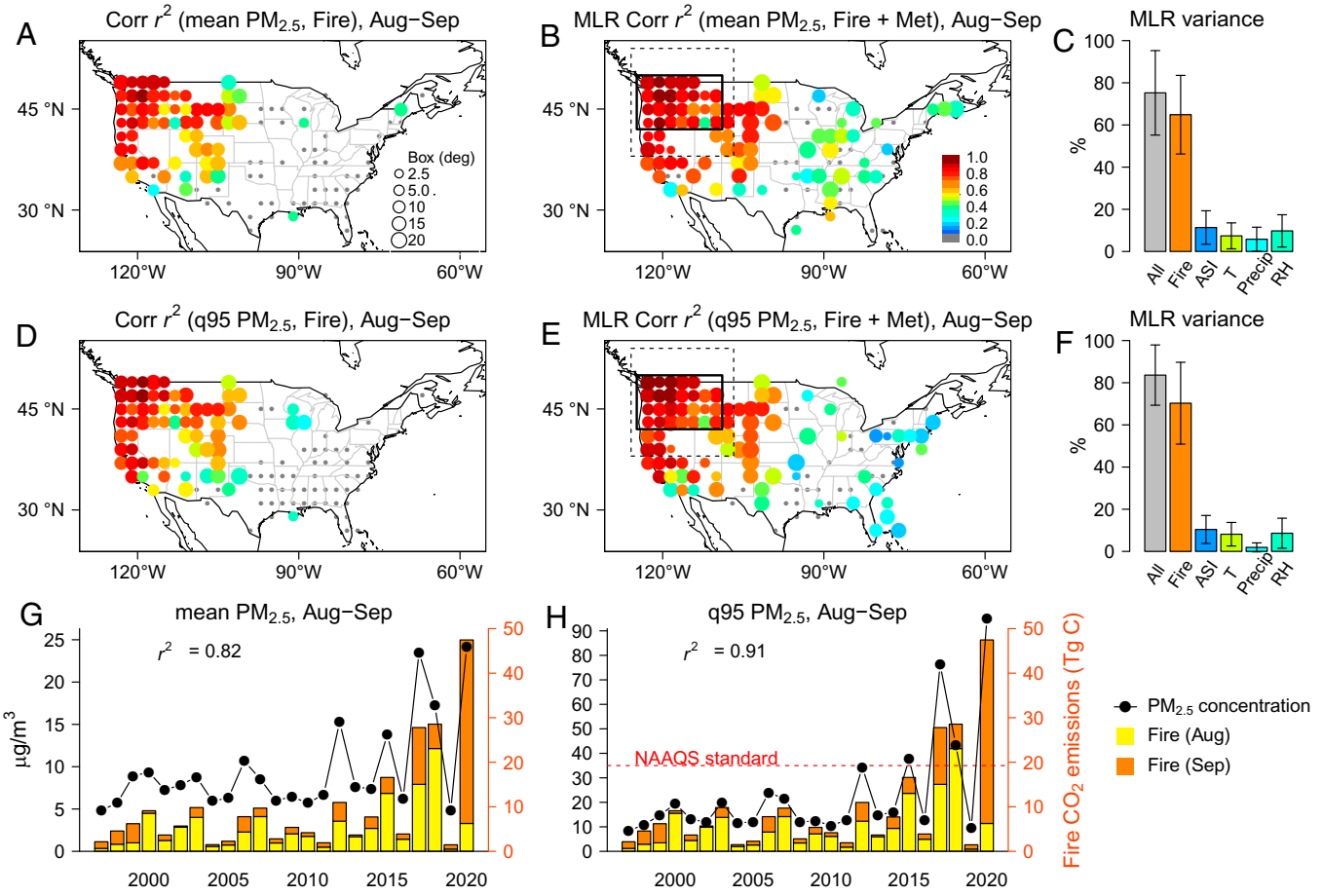

Fig. 1. Observed correlations between fires and surface $PM_{2.5}$ air quality. (*A–C*) Correlation (Corr) r^2 of mean $PM_{2.5}$ averaged over each 2° × 2° grid with regional total CO_2 emissions from fires in August (Aug) through September (Sep) during 1997–2020 derived from simple linear regression (*A*) versus MLR with consideration of meteorological (Met) variables (*B*) and the variance explained over the US Pacific Northwest (solid black box in *B*) by each predicting variable (*C*). The width of the box (in degrees [deg]), within which regional total fire emissions are best correlated with $PM_{2.5}$ at that site, is given in the right corner in *A*. The r^2 values are color-coded for sites with significant correlations, with gray indicating sites with insignificant correlations ($P > 0.05$). (*D–F*) Same as *A–C*, but for the q95 of available daily $PM_{2.5}$ observations at each grid in August through September. (*G* and *H*) Time series of the mean and q95 $PM_{2.5}$ in August through September averaged over US Pacific Northwest sites from 1997 to 2020, along with regional total CO_2 emissions from fires integrated over western North America (dashed black box in *B*). Precip, precipitation; RH, relative humidity; T, temperature; ASI, air stagnation index.

(QFED2.5) (63). Observations show hotspots of burned area and fire CO_2 emissions over the Pacific Northwest in August and September (Fig. 2 *A* and *B*). We investigate the extent to which models capture the interannual variability of fires over this region relative to their respective mean state. Evaluating normalized interannual variability provides insights into the sensitivity of simulated fires to meteorological and climatic variability, which is critical to establish the robustness of projected fire responses to climate change.

We first examine the land-only experiments driven by observation-based meteorological forcings to allow direct comparison with the observed fires in space and time (*Materials and Methods*). The land-only simulations generally capture the observed normalized interannual variability of burned area (r^2 = 0.32 to 0.67) and fire CO_2 emission (r^2 = 0.25 to 0.60) over western North America (Fig. 2 *C* and *D*), despite mean-state biases (*SI Appendix*, Fig. S3). Above-normal fire activity is observed and simulated in years such as 1988, 2006, 2012, 2017, 2018, and 2020, associated with severe drought conditions (64–69). The CESM2 model performs best in simulating the interannual variability of burned area (r^2 = 0.67; $P < 0.01$) and fire CO_2 emission (r^2 = 0.60 to 0.64; $P < 0.01$). For comparison, the correlations for burned area are r^2 = 0.49 ($P < 0.01$) for CNRM-ESM2-1 and r^2 = 0.32 ($P < 0.05$) for GFDL-ESM4.1. The amplitude of the observed interannual variability of fire CO_2 emissions (represented as SD in Fig. 2) is also best captured by CESM2: SD = 36.4%, compared to SD = 55.9 to 56.2% in observations, SD = 28.3% in GFDL-ESM4.1, and 20.6% in CNRM-ESM2-1.

The fully coupled ocean–land–atmosphere experiments allow us to project future fires under varying climate change scenarios. These coupled model simulations are driven by model-generated climate and thus are not expected to capture the timing and location of the observed fires during historical periods. Therefore, we evaluate the hemispheric to regional patterns in burned area and fire CO_2 emissions, as well as the strength of interannual variability during the 2000–2014 period. Both the land-only and coupled experiments from all three models simulate the salient features of the spatial patterns of burned area and fire CO_2 emissions across the Northern Hemisphere, such as capturing fire hotspots over western North America and Mediterranean Europe in August and September (*SI Appendix*, Figs. S4–S7). The models simulate reasonable fire interannual variability over these hotspot areas, despite large mean-state biases. Over western North America, total fire CO_2 emissions in August and September are overestimated by a factor of 2 in CESM2 and factors of 4 to 5 in GFDL-ESM4.1 and CNRM-ESM2-1, compared to the estimates from two satellite-based fire emission inventories

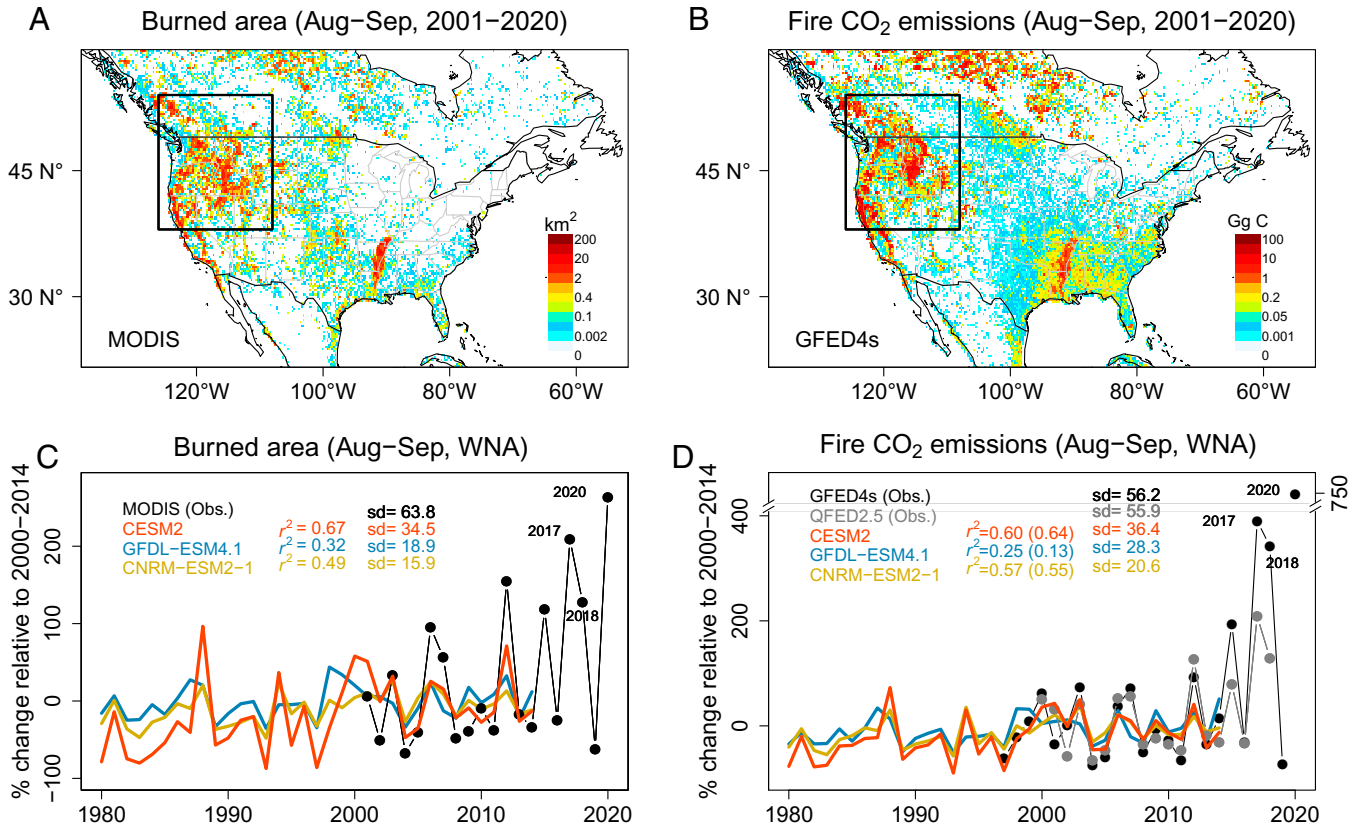

Fig. 2. Evaluating model simulations of fires over western North America. (*A* and *B*) The 2001–2020 climatology of August (Aug) through September (Sep) total burned area from MODIS satellite observations and fire CO_2 emissions from GFED4s over North America. (*C*) The relative changes of August through September total burned area over western North America (WNA; black box on map) from 1980 to 2020 versus 2000–2014 averages from MODIS satellite observations (black) and from three CMIP6 land-only experiments (solid lines). (*D*) Same as *C*, but for fire CO_2 emissions from two satellite-based inventories (black for GFED4s and gray for QFED2.5) and from three CMIP6 land-only experiments (solid lines). SDs (in percentages) and correlations r^2 between models and observational datasets (QFED2.5 in parentheses) are shown in *C* and *D*.

(*SI Appendix*, Fig. S3*B*). Similar high biases have previously been identified in CMIP5 Earth System Models (23, 41) and by the CMIP6 Fire Model Intercomparison Project (40). These studies suggest possible biases in the simulated fuel load (biomass), fire response to human activities, and fuel consumption rate applied in the models (40, 41, 70).

We conclude that the three CMIP6 Earth System Models have moderate ability to simulate changes in fire emissions in response to variations in climate and vegetation, despite varying levels of mean-state biases. To gauge the uncertainties of our $PM_{2.5}$ predictions associated with these biases, we compare MLR predictions driven by the relative changes of fire CO_2 emissions versus those driven by the absolute emission changes in each model. For CESM2, with small mean-state biases in historical fire CO_2 emissions, we find an overall consistent magnitude of western US mean $PM_{2.5}$ predictions between the two MLR models (*SI Appendix*, Fig. S8 *A* and *B*). For GFDL-ESM4.1 and CNRM-ESM2-1, with high mean-state biases in historical fire CO_2 emissions, the MLR model driven by the absolute changes of fire emissions predicts much larger $PM_{2.5}$ in 2080–2020, with the $PM_{2.5}$ prediction driven by relative changes agreeing better with that driven by the CESM2 model (*SI Appendix*, Fig. S8 *C*–*F*). Thus, we conclude that it is more reasonable to use the relative change of fire CO_2 emissions to drive the MLR prediction of future $PM_{2.5}$ levels.

Changes in Climate and Fires in the 21st Century. We next investigate changes in climate and fires over western North America in the 21st century from the CMIP6 coupled Earth system simulations under four climate change scenarios: SSP1-2.6 (low societal vulnerability combined with radiative forcing of 2.6 $W{\cdot}m^{-2}$ by 2100), SSP2-4.5 (intermediate societal vulnerability, 4.5 $W{\cdot}m^{-2}$ forcing), SSP3-7.0 (high societal vulnerability, 7.0 $W{\cdot}m^{-2}$ forcing), and SSP5-8.5 (fossil-fueled development, high emissions, 8.5 $W{\cdot}m^{-2}$ forcing) (71, 72). While studies have suggested that fire seasonality may change in a warming climate (73–75), our MLR model predictions build upon the strong correlation between $PM_{2.5}$ and fires during August through September over the Pacific Northwest under present-day climate. To investigate whether it is reasonable to focus on August through September under future climate, we examine fire seasonality and spatial pattern over North America under SSP5-8.5 (Fig. 3).

All three models project a lengthening of the fire season over the Pacific Northwest in a warmer climate, with elevated fire CO_2 emissions spanning from May to November during 2080–2100 under SSP5-8.5 compared to July to October at present (Fig. 3*A*). Nevertheless, all three models suggest that fire CO_2 emissions in the late 21st century peak in August and September, similar to the current climate. Therefore, we continue to focus our projections on changes in fires and $PM_{2.5}$ air quality in August and September. During August and September, fire CO_2 emissions are projected to increase significantly ($P < 0.05$) over western North America (Fig. 3*B*) and Mediterranean Europe (*SI Appendix*, Figs. S9 and S10) in the late 21st century under SSP5-8.5, according to our multiensemble and multimodel projections. These regions are particularly susceptible to water scarcity in a warming climate (76, 77), which could impact regional air quality via vegetation feedbacks (78).

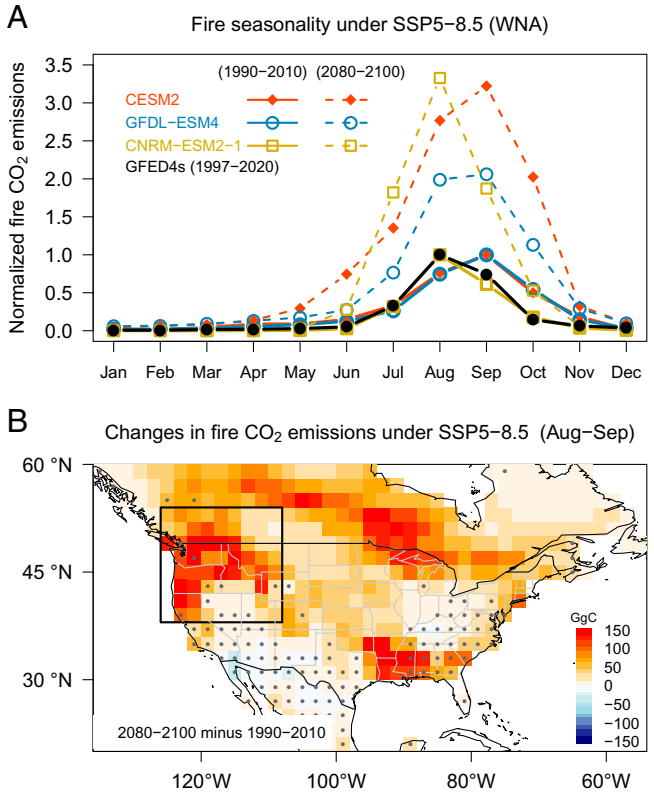

Fig. 3. Changes in fire seasonality in the late 21st century. (*A*) Monthly mean fire CO_2 emissions over western North America (WNA) under present day (1990–2010, solid lines) and SSP5-8.5 (2080–2100, dashed lines) normalized by the month with peak emissions at present day from CMIP6 coupled model experiments. Also shown are satellite-based estimates for the present-day climate (black). (*B*) Multimodel and multiensemble mean changes in CO_2 emissions from fires (in Gg C) in August (Aug) through September (Sep) during the late 21st century under SSP5-8.5 (2080–2100 minus 1990–2010). The results are first averaged across the available ensemble members from each model (three for CESM2, one for GFDL-ESM4.1, and five for CNRM-ESM2-1) and then averaged across the models. Stippling indicates grids with less than two models that show statistically significant ($P < 0.05$) changes or where the three models do not agree in sign. For each model, a change is defined as significant if >50% of the ensemble changes are statistically significant ($P < 0.05$).

Fig. 4 illustrates the temporal evolution of surface temperature, soil moisture, vegetation carbon mass, burned area, and fire CO_2 emissions from CESM2, which best simulates the observed interannual variability of fires, as discussed previously (Fig. 2). Changes in fire CO_2 emissions and burned area from the other two models are also shown for comparison. CESM2 projects an ∼2 K increase in August through September mean surface temperature over western North America by the 2040s (versus present day), with little difference across the SSPs (Fig. 4*A*). Surface temperatures among scenarios diverge afterward, with a 7.5 K increase under SSP5-8.5 compared to a 2 K increase under SSP1-2.6 by the late 21st century (versus present day). Following climate warming and rising CO_2 concentrations, which stimulates vegetation growth, CESM2 simulates a decrease in surface soil moisture and an increase in vegetation carbon mass (Fig. 4 *B* and *C*), both providing more favorable conditions for fires. Under the SSP3-7.0 and SSP5-8.5 high-warming scenarios, CESM2 projects an ∼10% decrease in surface soil moisture by the end of the 21st century. The projected decrease is consistent with the overall drying trend projected by 13 CMIP6 models (79), attributed primarily to enhanced evaporative demand and water use by vegetation in a warmer climate (80). Vegetation carbon mass shows an ∼50% increase by 2100 under SSP5-8.5, partly driven by CO_2 fertilization, increased temperature, and land-use changes (81–83).

Following the projected trends in climate and vegetation, CESM2 shows 50 to 120% increases in burned area and 110 to 250% increases in fire CO_2 emissions among different SSPs by 2100 over western North America (Fig. 4 *D* and *G* and *SI Appendix*, Table S2). The different increases in fires among the scenarios reflect impacts from both climate and population distributions (37). The projected increases in fire CO_2 emissions are ∼250% under the SSP3-7.0 and SSP5-8.5 extreme warming scenarios, more than twice that under the SSP1-2.6 climate-mitigation scenario. We note a smaller increase in fire burned area under SSP5-8.5 (100%) compared to SSP3-7.0 (120%) (red versus yellow lines in Fig. 4*G*). This may be related to the larger population projected under SSP5-8.5 (84) and thus stronger effects of fire suppression (85, 86). The influence of population density on fire suppression is also evident in historical simulations (*SI Appendix*, Fig. S11). Across all scenarios, the projected increases in fire CO_2 emissions are about twice those in burned area (Fig. 4), indicating increased emission efficiency per area burned, driven partly by increased vegetation biomass or increased fire duration in a warming climate.

All three models project substantial increases in burned area and fire CO_2 emissions in the late 21st century, although the magnitudes of the projected changes, the spatial patterns, and the spreads across scenarios and across ensemble members differ (Fig. 4 and *SI Appendix*, Figs. S9 and S10). The projected percentage increase in fire CO_2 emissions per degree warming is ∼40% in CESM2 and GFDL-ESM4.1 and ∼20% in CNRM-ESM2-1. Under SSP5-8.5, by the late 2100s, the projected increase in fire CO_2 emissions over western North America is 260% from GFDL-ESM4.1, 240% from CESM2, and 130% from CNRM-ESM2-1 (Fig. 4 *D*–*F*). GFDL-ESM4.1 shows the largest cross-scenario spread, with a 70% increase in fire CO_2 emissions under SSP1-2.6 and a 260% increase under SSP5-8.5 by the late 21st century (Fig. 4*E*). Among the three models, CNRM-ESM2-1 has the simplest fire module, but has the greatest number of ensembles (*Materials and Methods* and *SI Appendix*, Table S1). The larger ensemble spread for both historical and future simulations in CNRM-ESM2-1 results in a better estimate of the influence of the internal climate variability on fire emissions. There are also some intermodel differences in the spatial distribution of the projected fire increases over western North America (*SI Appendix*, Figs. S9 and S10). CESM2 shows larger increases of fire-burned area and emissions over the northern Great Plains, while CNRM-ESM2-1 and GFDL-ESM4.1 simulate larger increases over the Pacific Northwest. These results highlight the importance of multimodel and multiensemble projections to access uncertainties.

Comparison with Previous Studies. A few prior studies have estimated changes in fire emissions in the 21st century. Here, we present a brief comparison with our results. Under SSP2-4.5, by midcentury, the three CMIP6 models we consider projected a 60 to 80% increase in fire emissions over western North America. Our projected changes are smaller than the ∼150% increase projected by a statistical fire model considering impacts from climate, but not land use and population density (26). This is consistent with the smaller increase in fire carbon emissions over western North America during the 1960s to the 2010s from the CESM2 coupled historical simulations using interannually varying versus fixed-1850 land use and population density (*SI Appendix*, Fig. S11). Increased population

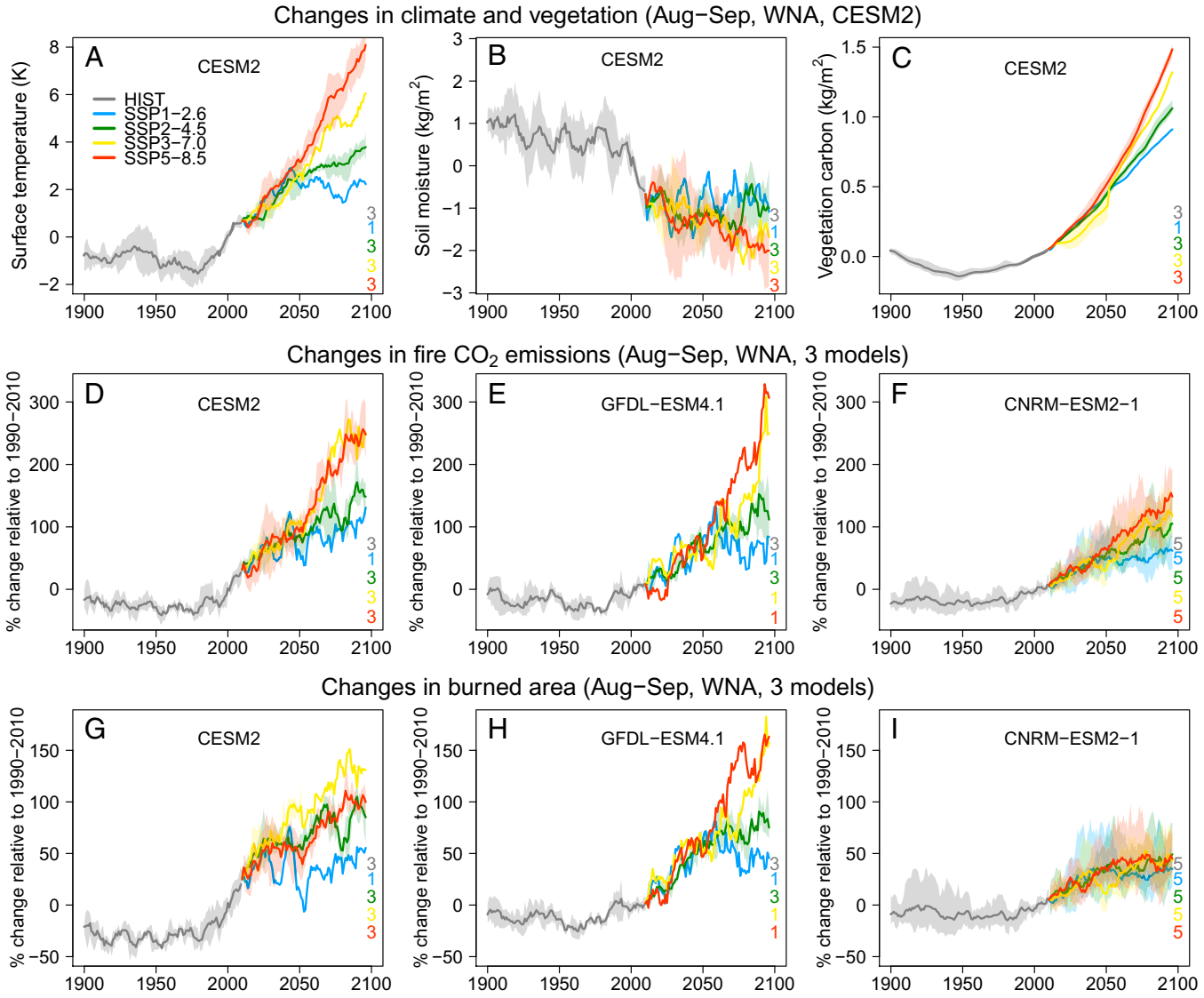

Fig. 4. Changes in climate and fires during August (Aug) through September (Sep) in the 21st century. Changes in 10-y running average of surface temperature (*A*), soil moisture in top 10 cm (*B*), and carbon mass in vegetation (*C*) relative to the 1990–2010 averages in August through September over western North America (WNA) from CESM2 historical simulations (gray) and future projections (colors) under four SSPs (*SI Appendix*, Table S1). (*D–I*) Same as *A*, but for total fire emissions of CO_2 (in percent) (*D–F*) and burned area (in percent) (*G–I*) from three CMIP6 Earth System Models: CESM2 (*Left*), GFDL-ESM4.1 (*Center*), and CNRM-ESM2-1 (*Right*). Thick lines represent the multiensemble mean, with shading illustrating the spread of available ensemble members (numbers denoted at the bottom-right corner of each graph).

density leads to greater fire suppression, wood harvest, and conversion of natural land (i.e., forest) to managed land (i.e., cropland), resulting in reduced forest biomass available for burning (40, 43, 87). Our projection of a 60 to 80% increase in fire CO_2 emissions over western North America is higher than the 45% increase projected by an offline process-based fire model driven by archived meteorological fields (23). The larger changes from our projection may be related to a positive feedback between fire and climate, e.g., increased fire risk due to enhanced surface temperature caused by fire-induced damage in vegetation canopy, which is not included in the offline simulation (37, 42, 88). The comparisons suggest that it is important to consider the impacts from climate, land use, and population influence for a robust projection of fires and feedbacks.

Increasing $PM_{2.5}$ Pollution from Wildfires in a Warming Climate. Changes in fire CO_2 emissions and meteorology projected by three CMIP6 Earth System Models are used to drive the MLR model to predict $PM_{2.5}$ over the western United States under four SSP scenarios (Fig. 5 and *SI Appendix*, Table S2). The MLR model driven by historical fires generally captures the observed variability and increasing trend of western US $PM_{2.5}$ in August through September during 1997–2020, demonstrating the credibility of the MLR-based $PM_{2.5}$ estimations (red versus black lines in Fig. 5 *D–F*). The MLR model driven by simulated future fires projects August through September mean $PM_{2.5}$ levels at western US sites to increase by ∼50% in the coming decades (2020–2050), even under the SSP1-2.6 strong-mitigation scenario with global CO_2 emissions cut severely and reaching net-zero around 2050. Under the "middle-of-the-road" SSP2-4.5 scenario, CO_2 emissions hover around current levels before falling midcentury, but do not reach net-zero by 2100 (71, 72); wildfire emissions and resulting $PM_{2.5}$ pollution would continue to increase after 2050 and almost double by 2100 compared to present-day levels (green lines in Figs. 4 *D–F* and 5 *D–F*). Under SSP5-8.5, with CO_2 emissions roughly double present

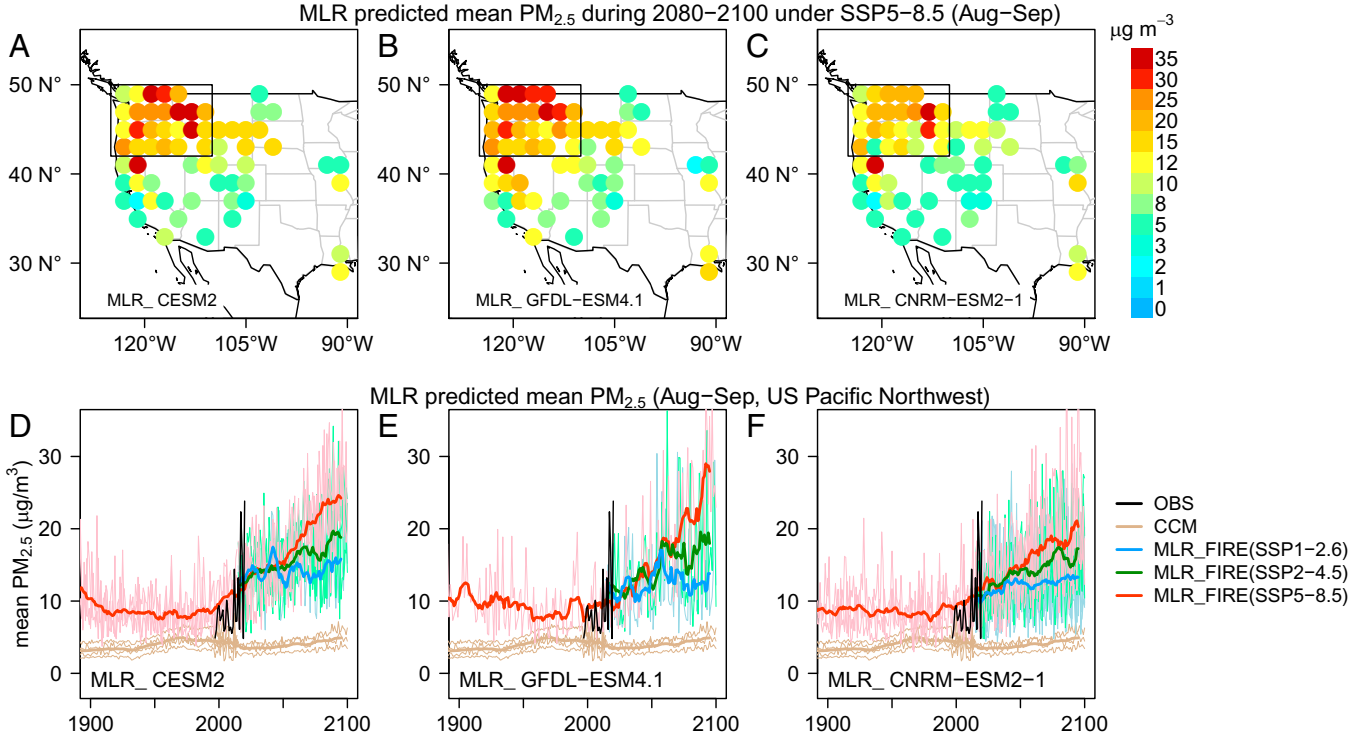

Fig. 5. Projected changes in August (Aug) through September (Sep) mean $PM_{2.5}$ due to increasing fire emissions. (*A–C*) The August through September mean $PM_{2.5}$ in 2080–2100 at western US sites (averaged over a 2° × 2° grid) predicted by MLR driven by fires from three CMIP6 models under SSP5-8.5. Only grids with MLR correlation $r^2 > 0.5$ are shown. (*D–F*) Temporal evolution of August through September mean $PM_{2.5}$ averaged over US Pacific Northwest sites (box on map) during 1900–2100 from the chemistry-climate model (CCM) simulations with prescribed fire emissions (tan lines) versus from the MLR model predictions, considering the impacts of future climate change on fire emissions under SSP1-2.6 (blue lines), SSP2-4.5 (green lines), and SSP5-8.5 (red lines). Thick lines represent 10-y running multiensemble averages, and thin lines represent averages for individual years from each ensemble member of each model (three for CESM2, one for GFDL-ESM4.1, and five for CNRM-ESM2-1). The August through September interannual time series from observations (OBS; black lines) is also shown for comparison.

levels by 2050 (71, 72) and western US summer mean temperature rising 6 to 8 K by the end of the century (Fig. 4*A*), mean $PM_{2.5}$ levels resulting from increasing wildfires during August through September could double to triple compared to present-day levels (red lines in Fig. 5 *D–F*), reaching 15 to 45 μg/m^3 for the US Pacific Northwest and northern California by the late 21st century (Fig. 5 *A–C* and *SI Appendix*, Table S2). These $PM_{2.5}$ increases are primarily driven by marked increases in fire emissions in the warming climate (*SI Appendix*, Fig. S12), with a small contribution from increasing stagnation frequency (*SI Appendix*, Fig. S13).

In contrast, $PM_{2.5}$ simulated directly by chemistry-climate models, using prescribed fire emissions of aerosol precursors responding to changes in land use, but not climate (*Materials and Methods*), do not show significant changes (+7%) throughout the 21st century under SSP5-8.5 (tan lines in Fig. 5 *D–F*). The prescribed fire emissions show little trend over western North America during the 21st century (*SI Appendix*, Fig. S14). The minor changes in anthropogenic emissions from the combustion of fossil fuels over western North America are not accounted for in our MLR $PM_{2.5}$ predictions.

We next examine changes in $PM_{2.5}$ extremes predicted by our MLR model in response to enhanced fire activity under the intermediate-mitigation SSP2-4.5 and low-mitigation SSP5-8.5 scenarios (Fig. 6). We predict considerable deterioration of $PM_{2.5}$ air quality over the western US in the 21st century under SSP5-8.5, caused by fires. By 2080–2100, under SSP5-8.5, the q95 of daily $PM_{2.5}$ in August through September is 20 to 170 μg/m^3 at Pacific Northwest sites, with 72 to 96% (model spread) of the sites experiencing q95 $PM_{2.5}$ above the 35 μg/m^3 US national standard, 52 to 68% above the unhealthy level (55 μg/m^3), and 0 to 8% above the very unhealthy level (150 μg/m^3; Fig. 6 *A–C*). The q95 $PM_{2.5}$ in August through September averaged over US Pacific Northwest sites exceeds the 35 μg/m^3 US national standard by the mid-21st century under both SSP2-4.5 and SSP5-8.5 (Fig. 6 *D–F*). By the late 21st century, the estimated q95 $PM_{2.5}$ levels averaged over US Pacific Northwest sites in individual models and ensembles could reach as much as 85 to 125 μg/m^3 under SSP2-4.5 and 115 to 155 μg/m^3 under SSP5-8.5.

Large fires burning across the US West in 2017, 2018, 2020, and 2021 caused historic levels of air pollution, loss of human life, and property damage (12, 54, 56). Unhealthy to hazardous concentrations of $PM_{2.5}$ (55 to 500 μg/m^3) were recorded at sites in the US Pacific Northwest and California for extended periods during summer to fall (11, 12). We use extreme value theory to examine whether these historically consequential events are more likely to occur in a future climate under intermediate- and high-emissions scenarios (*Materials and Methods*). We analyze large samples of q95 $PM_{2.5}$ at each site over the US Pacific Northwest during August through September from historical extremes (2017, 2018, and 2020), all historical observations for 1997–2020, and the MLR projections for 2080–2100 (Fig. 7). We find that the shape of the exceedance probability distribution of q95 $PM_{2.5}$ during the late 21st century under SSP5-8.5 resembles that for the historic $PM_{2.5}$ extremes of 2017, 2018, and 2020 caused by fires: ~70% of sites have q95 $PM_{2.5}$ exceeding the 35 μg/m^3 US national standard, compared to only 16% for average conditions observed during the

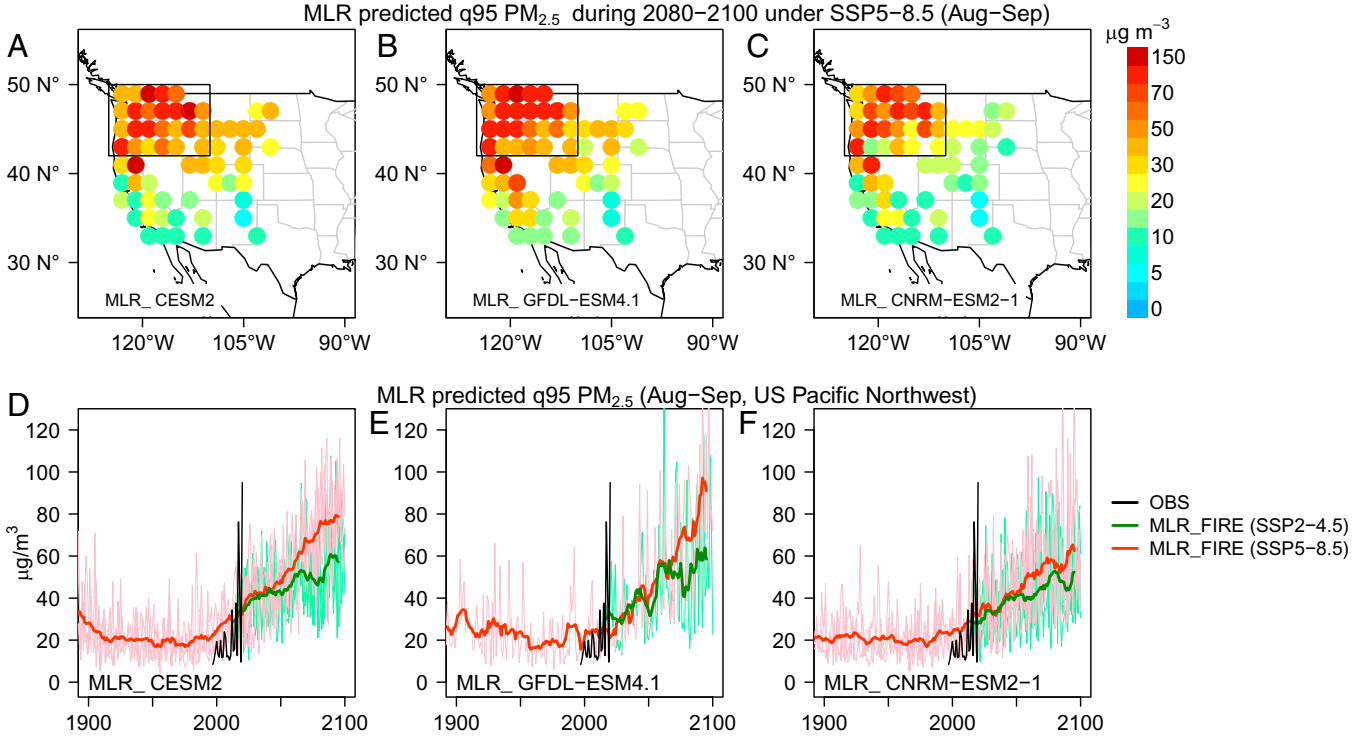

Fig. 6. Projected changes in $PM_{2.5}$ extremes in August (Aug) through September (Sep) due to increasing fires. (*A–C*) The q95 of daily $PM_{2.5}$ during August through September in 2080–2100 at western US sites (computed over a 2° × 2° grid) predicted by MLR driven by fires from three CMIP6 models under SSP5-8.5. Only grids with MLR correlation $r^2 > 0.5$ are shown. (*D–F*) Temporal evolution of the q95 $PM_{2.5}$ in August through September averaged over US Pacific Northwest sites (box on map) from the MLR model projections under SSP2-4.5 (green) and SSP5-8.5 (red). Thick lines represent 10-y running multiensemble averages, and thin lines represent averages for individual years from each ensemble member of each model (*SI Appendix*, Table S1). The August through September interannual time series from observations (OBS; black lines) is also shown for comparison.

past two decades (Fig. 7*A*). Under SSP2-4.5, the $PM_{2.5}$ distribution also shows a substantial shift toward extreme conditions. Fig. 7*B* shows the return period of the q95 $PM_{2.5}$ at US Pacific Northwest sites, fitted using a generalized extreme value distribution, from historical observations and the MLR $PM_{2.5}$ predictions. For a range of return periods (e.g., 5, 10, and 20 y), the estimated q95 $PM_{2.5}$ would double to triple in the MLR projections compared with historical observations. The return period of the recent pollution extremes of 2017, 2018, and 2020 (with a mean August through September q95 $PM_{2.5}$ of 72 μg/m^3) would decrease to ∼5 y in the late 21st century under SSP2-4.5 and to 3 y under SSP5-8.5.

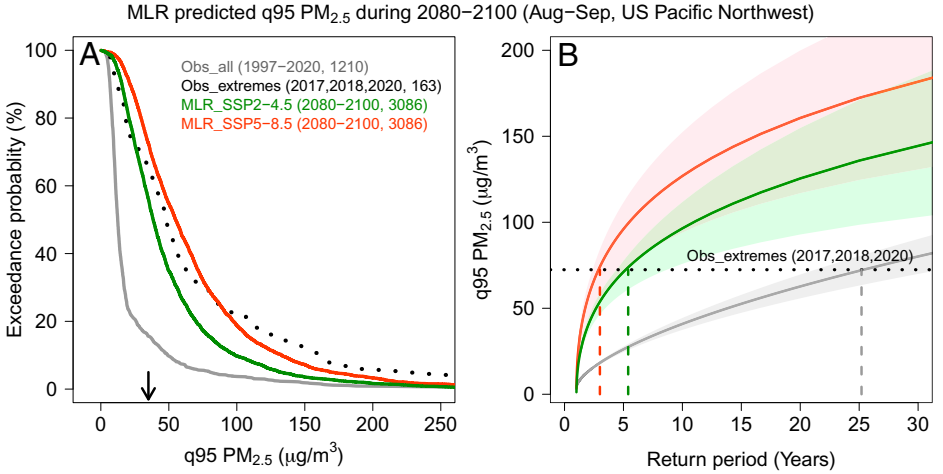

Fig. 7. Likelihood of historical pollution extremes in a warming climate. (*A*) Exceedance probability of the q95 of daily $PM_{2.5}$ at US Pacific Northwest sites during August (Aug) through September (Sep): from observations during 1997–2020 (gray solid line) and during the 2017, 2018, and 2020 extreme fire seasons (black dotted line), from the MLR $PM_{2.5}$ predictions driven by fires in three CMIP6 models during 2080–2100 under SSP2-4.5 (green) and SSP5-8.5 (red). The arrow denotes the 35 μg/m^3 US National Ambient Air Quality Standard for 24-h average $PM_{2.5}$. Numbers in brackets represent sample size for calculating the exceedance probability. (*B*) Return period of the q95 of daily $PM_{2.5}$ at US Pacific Northwest sites in August through September fitted using generalized extreme value distribution from observations during 1997–2020 (black solid line) and from the MLR $PM_{2.5}$ predictions driven by fires in three CMIP6 models during 2080–2100 under SSP2-4.5 (green) and SSP5-8.5 (red). The q95 of daily $PM_{2.5}$ in August through September of 2017, 2018, and 2020 is marked as the horizontal dotted line. Shading for observations represents the 95% CIs of estimated $PM_{2.5}$ levels for different return periods. Shading for MLR projections represents the maximum and minimum of estimated $PM_{2.5}$ levels for different return periods from different model ensembles. Intercepts between the horizontal black dotted line and the fitted solid lines represent the return periods for the observed 2017–2020 extremes in present and future climates.

Conclusions and Implications

Using an empirical statistical model driven by observations and CMIP6 Earth System Model projections of fire CO_2 emissions and meteorology, we project western US $PM_{2.5}$ air quality in the 21st century under a suite of SSPs. Late summer to fall $PM_{2.5}$ pollution over the US Pacific Northwest is projected to double to triple by 2080–2100 due to enhanced fire activity associated with drought and increased biomass under intermediate (SSP2-4.5) and high warming scenarios (SSP5-8.5). Even with strong mitigation under SSP1-2.6, western US $PM_{2.5}$ pollution would increase ∼50% by midcentury. The occurrence of four severe fire years in quick succession during 2017–2021 over the western US raises the possibility that climate change is already driving strong changes in fire regimes that may be underestimated by our models. Our study suggests that severe $PM_{2.5}$ air pollution caused by these historic fire events could occur every 5 y in the late 21st century under an intermediate climate change scenario (SSP2-4.5). Air quality exceedances caused by wildfires can be classified as "exceptional events," which are not counted toward a nonattainment determination, according to the US Environmental Protection Agency. However, a considerable increase in the frequency of fire-driven exceedances may complicate this policy, as these events become a new norm in the changing climate. The large spread across climate change scenarios highlights the cobenefits of climate mitigation for wildfires and air pollution. Multiagency collaborations, addressing climate mitigation, air quality, and forest management, are needed to minimize the adverse health impacts projected to result from fire smoke.

Materials and Methods

Multiple Linear Regression Model. The MLR model is developed using observational datasets of surface $PM_{2.5}$ concentrations, meteorological variables, and fire CO_2 emissions over western North America during 1997–2020. This observation-based MLR model is then applied to predict future $PM_{2.5}$ levels driven by fire CO_2 emissions and meteorology projected by the CMIP6 Earth System Models. Considering that climate model projections are more robust on larger scales, all observational datasets and CMIP6 model fields used for the MLR analysis are averaged onto a 2° × 2° grid. The MLR model predicts the mean and the q95 of $PM_{2.5}$ at each 2° × 2° grid d and month i in the form of:

$$PM2.5_{d,i}(t) = \beta_{d,i}Fire_{d,i}(t) + \sum_{k=1}^{4}\beta_{d,i,k}Met_{d,i,k}(t) + b_{d,i}, \quad [1]$$

where Fire(t) is the anomaly time series of fire CO_2 emissions in percentage relative to the present-day climatology, Met(t) is the anomaly time series of meteorological variables (i.e., surface temperature, precipitation, relative humidity, and air stagnation) relative to the present-day climatology; and β and b are regression coefficients fitted by the MLR. We select these four meteorological variables that have been previously identified to be correlated with surface $PM_{2.5}$ (11, 52). We perform the regression by adding and deleting prediction parameters stepwise to obtain the best fit based on the Akaike Information Criterion. The relative importance of each predictor is determined by using a bootstrap approach described in ref. 92. The performance of the MLR model is tested by using leave-one-out cross-validation (*SI Appendix*, section S1).

The observation-based MLR model is applied to predict mean and the q95 of surface $PM_{2.5}$ concentrations at each 2° × 2° grid, driven by monthly time series of fire CO_2 emissions and meteorology projected by the CMIP6 Earth System Models under a suite of climate change scenarios over the course of the 21st century. To ensure that we only apply the MLR predictions at locations where $PM_{2.5}$ levels are primarily driven by fire emissions, we limit our analysis to western US grid cells where the observed correlation r^2 from the MLR model is greater than 0.5 during August and September; as such, sites located in urban areas with large anthropogenic influence are filtered out. For $PM_{2.5}$ prediction at each valid grid, we calculate the anomaly time series (in percentage relative to the present-day 1990–2010 climatology) of total fire CO_2 emissions in a projected future climate, integrated over a regional box where the maximum correlation with $PM_{2.5}$ is found based on historical observations (Fig. 1). This approach thus accounts for the influence of regional smoke transport. Anomaly time series of meteorological variables in the future climate are calculated as the absolute differences from the present-day 1990–2010 climatology for each valid 2° × 2° grid.

Observational Datasets. Daily observations of $PM_{2.5}$ at surface-monitoring sites during 1997–2020 are obtained from the US Environmental Protection Agency's Air Quality System (https://www.epa.gov/aqs). To maximize data availability, we include $PM_{2.5}$ measured with both the Federal Reference Methods and non-Federal Reference Methods, as a strong linear correlation ($r^2 = 0.92$) between these two methods has been found at colocated monitors (93). To be consistent with the other datasets used for the MLR analysis, as well as to increase the statistical power and robustness of the analysis, we average all available daily surface $PM_{2.5}$ observations onto a 2° × 2° grid. For each month at each 2° × 2° grid cell, we calculate the average and the q95 of available daily $PM_{2.5}$ from all sites within that grid. Most grids have sample sizes of 50 to 200 daily $PM_{2.5}$ observations each month; only grids with at least 20 samples per month are considered in our analyses (*SI Appendix*, Fig. S2).

To represent the intensity and severity of wildfires, we use satellite observations of burned area and satellite-based estimations of fire CO_2 emissions, consistent with the datasets available from the CMIP6 fire models. The monthly burned area is from the Collection 6 MODIS climate model grid burned-area product (2000–2020, 0.25° × 0.25°) (60). Fire emissions of CO_2 are obtained from the Global Fire Emissions Dataset Version 4 with small fires (GFED4s; 1997–2020, 0.25° × 0.25°) based on satellite-retrieved burned area (61, 62) and the Quick Fire Emission Dataset Version 2.5 (QFED2.5; 2000–2019, 0.1° × 0.1°) based on satellite-observed fire radiative power (63). The MLR model only uses fire CO_2 emissions from GFED4s averaged onto a 2° × 2° grid, while both GFED4s and QFED2.5 are used to evaluate the CMIP6 fire models.

The MLR analysis includes four meteorological variables that have been previously identified to have correlations with surface $PM_{2.5}$ (11, 52): surface temperature, precipitation, relative humidity, and air stagnation (*SI Appendix*, section S2). Monthly mean surface temperature, precipitation, and relative humidity are obtained from the European Centre for Medium-Range Weather Forecasts Reanalysis Version 5 (1997–2020, 0.1° × 0.1°) (94). The air stagnation index is obtained from the US National Centers for Environmental Information (95). All original datasets are averaged onto a 2° × 2° grid for the MLR analysis.

CMIP6 Fire Models. We use simulations from three CMIP6 Earth System Models (CESM2, GFDL-ESM4.1, and CNRM-ESM2-1) that archived CO_2 emissions from fires and meteorological variables needed for the MLR model. The models' horizontal resolutions range from 1.0° to 1.5° (*SI Appendix*, Table S1). Vegetation structure and functioning in all three models (e.g., leaf area index) respond to changes in climate. GFDL-ESM4.1 simulates daily vegetation distribution (58, 96–98), while CESM2 and CNRM-ESM2-1 use prescribed land use and land cover change files (49, 59). Fire CO_2 emissions in all three CMIP6 models are simulated dynamically, coupled to climate and vegetation (*SI Appendix*, section S3) (42, 43, 45–47, 50, 51, 99). However, these models do not calculate fire emissions of particles or non-CO_2 gases, so atmospheric chemistry in these models is not coupled to interactive fire emissions responding to climate change.

Two sets of experiments from these models are used: 1) land-only experiments (LAND-HIST experiment from the Land Use Model Intercomparison) driven by the observation-based meteorological forcings (derived from dynamic downscaling of the 20th-Century Reanalysis) (100, 101); and 2) coupled land–atmosphere–ocean historical simulations (CMIP6 HIST experiment) and future projections (from the Scenario Model Intercomparison Project) driven by emissions of greenhouse gases and aerosols under four SSPs: SSP1-2.6, SSP2-4.5, SSP3-7.0, and SSP5-8.5 (71). The land-only experiments driven by observed climate allow for direct comparison with observations in space and time in order to understand biases related to the modeling of fire dynamics (Fig. 2). The coupled model simulations are used to understand changes in fires under climate change scenarios, which serve as a key predictor for future $PM_{2.5}$ levels (Figs. 5–7). To understand the drivers of the temporal evolution of historical fires (*SI Appendix*, Fig. S11), we analyze three CESM2 coupled-model experiments: 1) with all historical forcings (HIST); 2) the control simulation with

preindustrial forcings, including constant land cover and land use, land management, and population density at 1850 levels (pi-Control) (102); and 3) with all historical forcings the same as HIST, but with land use held constant at 1850 levels, as in pi-Control (HIST_NoLU) (101).

Chemistry-Climate Model $PM_{2.5}$ Simulations Using Prescribed Fire Emissions. We compare the MLR-based estimations of $PM_{2.5}$ driven by interactive fires responding to climate change with $PM_{2.5}$ directly simulated by three chemistry-climate models (103–105). In these chemistry-climate models, fire emissions of particles are prescribed for both historical and future simulations. Historical simulations of these models use fire emissions of gases and particles from GFED4s for 1997–2014 and historical reconstructions from the Fire Model Intercomparison Project prior to 1997 (28, 48). Future fire emissions of gases and particles are prescribed based on the spatial distribution of the 2005–2014 climatology from GFED4s and consider the impacts from land use, but not climate change (29). There are no substantial trends or interannual variability in biomass burning emissions of aerosols used for future $PM_{2.5}$ projections from these chemistry-climate models (*SI Appendix*, Fig. S14). Future $PM_{2.5}$ levels simulated by these chemistry-climate models thus reflect the impacts from changes in anthropogenic emissions and meteorology, but overlook the impact of climate-driven increases in fire emissions of aerosols and aerosol precursors.

Calculation of Exceedance Probability and Return Period. To examine how prevalent the recent $PM_{2.5}$ pollution extremes caused by fires in 2017, 2018, and 2020 may be in a warming climate, we compare the exceedance probability and return period of the q95 of daily $PM_{2.5}$ in August through September at US Pacific Northwest sites from historical observations with MLR projections under SSP2-4.5 and SSP5-8.5 scenarios.

The exceedance probability is calculated as $1 - F_n$, where F_n is the empirical cumulative distribution function, calculated as $F_n(t) = \frac{1}{n}\sum_{i=1}^{n} \mathbf{1}_{X_i \le t}$, where n is the total number of the predicted monthly q95 $PM_{2.5}$ at each site in the US Pacific Northwest in August and September. $\sum_{i=1}^{n} \mathbf{1}_{X_i \le t}$ is the number of events with the predicted q95 $PM_{2.5}$ smaller than a given q95 $PM_{2.5}$ level of t.

The return levels and return periods are estimated by using extreme value theory (106). Extreme value theory has been used in previous studies to estimate return levels and days of ozone pollution events under present and future climates (107–109). Here, in this study, we perform the extreme event analysis with the extRemes package in R (110) using large samples of q95 $PM_{2.5}$ at each site in the US Pacific Northwest during August through September from historical extremes (2017, 2018, and 2020), from all historical observations for 1997–2020, and from the MLR projections for 2080–2100. The observed and MLR-predicted q95 $PM_{2.5}$ are fitted by using a generalized extreme value distribution function. The 95% CIs are estimated based on the delta method using the parameter covariance (110).

Data Availability. All study data are included in the article and/or *SI Appendix*. The data from three CMIP6 models used in this study (89–91) are publicly available at https://esgf-node.llnl.gov/projects/cmip6/. Surface observations of $PM_{2.5}$, meteorological variables from reanalysis datasets, satellite observations of burned area, and fire-emission inventories are publicly available through the links provided at the corresponding references, as described in *Materials and Methods*.

ACKNOWLEDGMENTS. This study was supported by awards from the National Oceanic and Atmospheric Administration (NOAA), US Department of Commerce (NA14OAR4320106 and NA18OAR4320123). The statements, findings, conclusions, and recommendations are those of the authors and do not necessarily reflect the views of NOAA. R.S. acknowledges the European Union's Horizon 2020 research and innovation program under Grant Agreement 101003536 (ESM2025–Earth System Models for the Future). We thank Yan Yu, Songmiao Fan, and Wenhao Dong from NOAA Geophysical Fluid Dynamics Laboratory and two anonymous reviewers for their helpful comments on the manuscript.

Author affiliations: [a]Atmospheric and Oceanic Sciences, Princeton University, Princeton, NJ 08540; [b]National Oceanic and Atmospheric Administration Geophysical Fluid Dynamics Laboratory, National Oceanic and Atmospheric Administration, Princeton, NJ 08540; [c]Centre National de Recherches Météorologiques, Université de Toulouse, Météo-France, Centre National de la Recherche Scientifique, 31057 Toulouse, France; [d]Climate and Global Dynamics Laboratory, National Center for Atmospheric Research, Boulder, CO 80305; and [e]International Center for Climate and Environment Sciences, Institute of Atmospheric Physics, Chinese Academy of Sciences, Beijing 100029, China

1. US Environmental Protection Agency, Data from the 2017 National Emissions Inventory (2017). https://www.epa.gov/air-emissions-inventories/2017-national-emissions-inventory-nei-data. Accessed 20 March 2021.
2. D. M. J. S. Bowman *et al.*, Vegetation fires in the Anthropocene. *Nat. Rev. Earth Environ.* **1**, 500–515 (2020).
3. F. H. Johnston *et al.*, Estimated global mortality attributable to smoke from landscape fires. *Environ. Health Perspect.* **120**, 695–701 (2012).
4. M. Burke *et al.*, The changing risk and burden of wildfire in the United States. *Proc. Natl. Acad. Sci. U.S.A.* **118**, e2011048118 (2021).
5. G. P. Schill *et al.*, Widespread biomass burning smoke throughout the remote troposphere. *Nat. Geosci.* **13**, 422–427 (2020).
6. A. L. Westerling, H. G. Hidalgo, D. R. Cayan, T. W. Swetnam, Warming and earlier spring increase western U.S. forest wildfire activity. *Science* **313**, 940–943 (2006).
7. A. L. Westerling, Increasing western US forest wildfire activity: Sensitivity to changes in the timing of spring. *Philos. Trans. R. Soc. Lond. B Biol. Sci.* **371**, 20150178 (2016).
8. J. T. Abatzoglou, A. P. Williams, Impact of anthropogenic climate change on wildfire across western US forests. *Proc. Natl. Acad. Sci. U.S.A.* **113**, 11770–11775 (2016).
9. C. D. McClure, D. A. Jaffe, US particulate matter air quality improves except in wildfire-prone areas. *Proc. Natl. Acad. Sci. U.S.A.* **115**, 7901–7906 (2018).
10. K. O'Dell, B. Ford, E. V. Fischer, J. R. Pierce, Contribution of wildland-fire smoke to US $PM_{2.5}$ and its influence on recent trends. *Environ. Sci. Technol.* **53**, 1797–1804 (2019).
11. Y. Xie, M. Lin, L. W. Horowitz, Summer PM2.5 pollution extremes caused by wildfires over the western United States during 2017–2018. *Geophys. Res. Lett.* **47**, e2020GL089429 (2020).
12. R. J. Laing, D. A. Jaffe, Wildfires are causing extreme PM concentrations in the western United States. *The Magazine for Environmental Managers*, June (2019). pubs.awma.org/flip/EM-June-2019/jaffe.pdf. Accessed 20 March 2021.
13. P. Yu, R. Xu, M. J. Abramson, S. Li, Y. Guo, Bushfires in Australia: A serious health emergency under climate change. *Lancet Planet. Health* **4**, e7–e8 (2020).
14. S. Vardoulakis, B. B. Jalaludin, G. G. Morgan, I. C. Hanigan, F. H. Johnston, Bushfire smoke: Urgent need for a national health protection strategy. *Med. J. Aust.* **212**, 349–353.e1 (2020).
15. A. van Donkelaar *et al.*, Satellite-based estimates of ground-level fine particulate matter during extreme events: A case study of the Moscow fires in 2010. *Atmos. Environ.* **45**, 6225–6232 (2011).
16. T. J. Yasunari *et al.*, Extreme air pollution events in Hokkaido, Japan, traced back to early snowmelt and large-scale wildfires over East Eurasia: Case studies. *Sci. Rep.* **8**, 6413 (2018).
17. P. Crippa *et al.*, Population exposure to hazardous air quality due to the 2015 fires in Equatorial Asia. *Sci. Rep.* **6**, 37074 (2016).
18. C. E. Reid *et al.*, Critical review of health impacts of wildfire smoke exposure. *Environ. Health Perspect.* **124**, 1334–1343 (2016).
19. K. O'Dell *et al.*, Hazardous air pollutants in fresh and aged western US wildfire smoke and implications for long-term exposure. *Environ. Sci. Technol.* **54**, 11838–11847 (2020).
20. N. Borchers Arriagada *et al.*, Unprecedented smoke-related health burden associated with the 2019-20 bushfires in eastern Australia. *Med. J. Aust.* **213**, 282–283 (2020).
21. N. Fann *et al.*, The health impacts and economic value of wildland fire episodes in the U.S.: 2008-2012. *Sci. Total Environ.* **610-611**, 802–809 (2018).
22. US Environmental Protection Agency, Treatment of data influenced by exceptional events (2007). https://www.epa.gov/air-quality-analysis/final-2016-exceptional-events-rule-supporting-guidance-documents-updated-faqs. Accessed 20 March 2021.
23. B. Ford *et al.*, Future fire impacts on smoke concentrations, visibility, and health in the contiguous United States. *Geohealth* **2**, 229–247 (2018).
24. E. N. Stavros, J. T. Abatzoglou, D. McKenzie, N. K. Larkin, Regional projections of the likelihood of very large wildland fires under a changing climate in the contiguous Western United States. *Clim. Change* **126**, 455–468 (2014).
25. J. T. Abatzoglou, A. P. Williams, R. Barbero, Global emergence of anthropogenic climate change in fire weather indices. *Geophys. Res. Lett.* **46**, 326–336 (2019).
26. X. Yue, L. J. Mickley, J. A. Logan, J. O. Kaplan, Ensemble projections of wildfire activity and carbonaceous aerosol concentrations over the western United States in the mid-21st century. *Atmos Environ (1994)* **77**, 767–780 (2013).
27. J. S. Littell, D. McKenzie, H. Y. Wan, S. A. Cushman, Climate change and future wildfire in the western United States: An ecological approach to nonstationarity. *Earths Futur.* **6**, 1097–1111 (2018).
28. M. J. E. van Marle *et al.*, Historic global biomass burning emissions for CMIP6 (BB4CMIP) based on merging satellite observations with proxies and fire models (1750–2015). *Geosci. Model Dev.* **10**, 3329–3357 (2017).
29. L. Feng *et al.*, The generation of gridded emissions data for CMIP6. *Geosci. Model Dev.* **13**, 461–482 (2020).
30. Y. F. Lam, J. S. Fu, S. Wu, L. J. Mickley, Impacts of future climate change and effects of biogenic emissions on surface ozone and particulate matter concentrations in the United States. *Atmos. Chem. Phys.* **11**, 4789–4806 (2011).
31. W. J. Collins *et al.*, AerChemMIP: Quantifying the effects of chemistry and aerosols in CMIP6. *Geosci. Model Dev.* **10**, 585–607 (2017).
32. J. C. Liu *et al.*, Particulate air pollution from wildfires in the western US under climate change. *Clim. Change* **138**, 655–666 (2016).
33. M. Val Martin *et al.*, How emissions, climate, and land use change will impact mid-century air quality over the United States: A focus on effects at national parks. *Atmos. Chem. Phys.* **15**, 2805–2823 (2015).
34. D. V. Spracklen *et al.*, Wildfires drive interannual variability of organic carbon aerosol in the western U.S. in summer. *Geophys. Res. Lett.* **34**, L16816 (2007).
35. J. E. Neumann *et al.*, Estimating PM2.5-related premature mortality and morbidity associated with future wildfire emissions in the western US. *Environ. Res. Lett.* **16**, 035019 (2021).
36. D. Mills *et al.*, Projecting age-stratified risk of exposure to inland flooding and wildfire smoke in the United States under two climate scenarios. *Environ. Health Perspect.* **126**, 047007 (2018).

37. W. Knorr, L. Jiang, A. Arneth, Climate, CO_2 and human population impacts on global wildfire emissions. *Biogeosciences* **13**, 267–282 (2016).
38. S. Kloster, N. M. Mahowald, J. T. Randerson, P. J. Lawrence, The impacts of climate, land use, and demography on fires during the 21st century simulated by CLM-CN. *Biogeosciences* **9**, 509–525 (2012).
39. D. McKenzie, J. S. Littell, Climate change and the eco-hydrology of fire: Will area burned increase in a warming western USA? *Ecol. Appl.* **27**, 26–36 (2017).
40. F. Li *et al.*, Historical (1700–2012) global multi-model estimates of the fire emissions from the fire modeling intercomparison project (FireMIP). *Atmos. Chem. Phys.* **19**, 12545–12567 (2019).
41. S. Kloster, G. Lasslop, Historical and future fire occurrence (1850 to 2100) simulated in CMIP5 earth system models. *Global Planet. Change* **150**, 58–69 (2017).
42. F. Li, D. M. Lawrence, Role of fire in the global land water budget during the twentieth century due to changing ecosystems. *J. Clim.* **30**, 1893–1908 (2017).
43. D. S. Ward, E. Shevliakova, S. Malyshev, S. Rabin, Trends and variability of global fire emissions due to historical anthropogenic activities. *Global Biogeochem. Cycles* **32**, 122–142 (2018).
44. Y. Yu *et al.*, Increased risk of the 2019 Alaskan July fires due to anthropogenic activity. *Bull. Am. Meteorol. Soc.* **102**, S1–S7 (2021).
45. F. Li, X. D. Zeng, S. Levis, A process-based fire parameterization of intermediate complexity in a dynamic global vegetation model. *Biogeosciences* **9**, 2761–2780 (2012).
46. F. Li, B. Bond-Lamberty, S. Levis, Quantifying the role of fire in the Earth system–Part 2: Impact on the net carbon balance of global terrestrial ecosystems for the 20th century. *Biogeosciences* **11**, 1345–1360 (2014).
47. S. S. Rabin *et al.*, A fire model with distinct crop, pasture, and non-agricultural burning: Use of new data and a model-fitting algorithm for FINAL.1. *Geosci. Model Dev.* **11**, 815–842 (2018).
48. S. S. Rabin *et al.*, The Fire Modeling Intercomparison Project (FireMIP), phase 1: Experimental and analytical protocols with detailed model descriptions. *Geosci. Model Dev.* **10**, 1175–1197 (2017).
49. D. M. Lawrence *et al.*, The Community Land Model Version 5: Description of new features, benchmarking, and impact of forcing uncertainty. *J. Adv. Model. Earth Syst.* **11**, 4245–4287 (2019).
50. C. Delire *et al.*, The global land carbon cycle simulated with ISBA-CTRIP: Improvements over the last decade. *J. Adv. Model. Earth Syst.* **12**, e2019MS001886 (2020).
51. F. Li, S. Levis, D. S. Ward, Quantifying the role of fire in the Earth system–Part 1: Improved global fire modeling in the Community Earth System Model (CESM1). *Biogeosciences* **10**, 2293–2314 (2013).
52. A. P. K. Tai, L. J. Mickley, D. J. Jacob, Correlations between fine particulate matter (PM2.5) and meteorological variables in the United States: Implications for the sensitivity of PM2.5 to climate change. *Atmos. Environ.* **44**, 3976–3984 (2010).
53. D. A. Jaffe *et al.*, Wildfire and prescribed burning impacts on air quality in the United States. *J. Air Waste Manag. Assoc.* **70**, 583–615 (2020).
54. J. Balch *et al.*, Switching on the big burn of 2017. *Fire (Basel)* **1**, 17 (2018).
55. National Interagency Coordination Center, National Interagency Coordination Center Report on wildland fires and acres (2019). https://www.nifc.gov/fire-information/statistics/wildfires. Accessed 20 March 2021.
56. P. E. Higuera, J. T. Abatzoglou, Record-setting climate enabled the extraordinary 2020 fire season in the western United States. *Glob. Change Biol.* **27**, 1–2 (2021).
57. G. Danabasoglu *et al.*, The Community Earth System Model Version 2 (CESM2). *J. Adv. Model. Earth Syst.* **12**, e2019MS001916 (2020).
58. J. P. Dunne *et al.*, The GFDL Earth system model version 4.1 (GFDL-ESM 4.1): Overall coupled model description and simulation characteristics. *J. Adv. Model. Earth Syst.* **12**,, e2019MS002015 (2020).
59. R. Séférian *et al.*, Evaluation of CNRM Earth system model, CNRM-ESM2-1: Role of Earth system processes in present-day and future climate. *J. Adv. Model. Earth Syst.* **11**, 4182–4227 (2019).
60. L. Giglio, L. Boschetti, D. P. Roy, M. L. Humber, C. O. Justice, The collection 6 MODIS burned area mapping algorithm and product. *Remote Sens. Environ.* **217**, 72–85 (2018).
61. J. T. Randerson, Y. Chen, G. R. Werf, B. M. Rogers, D. C. Morton, Global burned area and biomass burning emissions from small fires. *J. Geophys. Res. Biogeosci.* **117**, G04012 (2012).
62. G. R. van der Werf *et al.*, Global fire emissions estimates during 1997–2016. *Earth Syst. Sci. Data* **9**, 697–720 (2017).
63. A. Darmenov, A. M. da Silva, The Quick Fire Emissions Dataset (QFED)–Documentation of versions 2.1, 2.2, and 2.4 (2015) ftp.as.harvard.edu/gcgrid/data/ExtData/HEMCO/QFED/v2018-07/. Accessed 20 March 2021.
64. M. Hoerling *et al.*, Causes and predictability of the 2012 Great Plains drought. *Bull. Am. Meteorol. Soc.* **95**, 269–282 (2014).
65. F. Kogan, W. Guo, 2006–2015 mega-drought in the western USA and its monitoring from space data. *Geomatics Nat. Hazards Risk* **6**, 651–668 (2015).
66. A. Hoell *et al.*, Anthropogenic contributions to the intensity of the 2017 United States northern Great Plains drought. *Bull. Am. Meteorol. Soc.* **100**, S19–S24 (2019).
67. D. LeComte, U.S. weather highlights 2018: Another historic hurricane and wildfire season. *Weatherwise* **72**, 12–23 (2019).
68. H. Wang, S. D. Schubert, R. D. Koster, Y. Chang, Attribution of the 2017 northern high plains drought. *Bull. Am. Meteorol. Soc.* **100**, S25–S29 (2019).
69. M. Lin, L. W. Horowitz, R. Payton, A. M. Fiore, G. Tonnesen, US surface ozone trends and extremes from 1980 to 2014: Quantifying the roles of rising Asian emissions, domestic controls, wildfires, and climate. *Atmos. Chem. Phys.* **17**, 2943–2970 (2017).
70. T. T. van Leeuwen *et al.*, Biomass burning fuel consumption rates: A field measurement database. *Biogeosciences* **11**, 7305–7329 (2014).
71. B. C. O'Neill *et al.*, The Scenario Model Intercomparison Project (ScenarioMIP) for CMIP6. *Geosci. Model Dev.* **9**, 3461–3482 (2016).
72. K. Riahi *et al.*, The shared socioeconomic pathways and their energy, land use, and greenhouse gas emissions implications: An overview. *Glob. Environ. Change* **42**, 153–168 (2017).
73. W. M. Jolly *et al.*, Climate-induced variations in global wildfire danger from 1979 to 2013. *Nat. Commun.* **6**, 7537 (2015).
74. K. L. Riley, R. A. Loehman, Mid-21st-century climate changes increase predicted fire occurrence and fire season length, Northern Rocky Mountains, United States. *Ecosphere* **7**, e01543 (2016).
75. E. K. Brown, J. Wang, Y. Feng, US wildfire potential: A historical view and future projection using high-resolution climate data. *Environ. Res. Lett.* **16**, 034060 (2021).
76. L. M. Rasmijn *et al.*, Future equivalent of 2010 Russian heatwave intensified by weakening soil moisture constraints. *Nat. Clim. Chang.* **8**, 381–385 (2018).
77. L. Samaniego *et al.*, Anthropogenic warming exacerbates European soil moisture droughts. *Nat. Clim. Chang.* **8**, 421–426 (2018).
78. M. Lin *et al.*, Vegetation feedbacks during drought exacerbate ozone air pollution extremes in Europe. *Nat. Clim. Chang.* **10**, 444–451 (2020).
79. B. I. Cook *et al.*, Twenty-first century drought projections in the CMIP6 forcing scenarios. *Earths Futur.* **8**, e2019EF001461 (2020).
80. J. S. Mankin, R. Seager, J. E. Smerdon, B. I. Cook, A. P. Williams, Mid-latitude freshwater availability reduced by projected vegetation responses to climate change. *Nat. Geosci.* **12**, 983–988 (2019).
81. R. A. Fisher *et al.*, Parametric controls on vegetation responses to biogeochemical forcing in the CLM5. *J. Adv. Model. Earth Syst.* **11**, 2879–2895 (2019).
82. S. Sitch *et al.*, Evaluation of the terrestrial carbon cycle, future plant geography and climate-carbon cycle feedbacks using five dynamic global vegetation models (DGVMs). *Glob. Change Biol.* **14**, 2015–2039 (2008).
83. Z. Zhu *et al.*, Greening of the Earth and its drivers. *Nat. Clim. Chang.* **6**, 791–795 (2016).
84. S. Kc, W. Lutz, The human core of the shared socioeconomic pathways: Population scenarios by age, sex and level of education for all countries to 2100. *Glob. Environ. Change* **42**, 181–192 (2017).
85. N. Andela *et al.*, A human-driven decline in global burned area. *Science* **356**, 1356–1362 (2017).
86. F. Li, D. M. Lawrence, B. Bond-Lamberty, Human impacts on 20th century fire dynamics and implications for global carbon and water trajectories. *Global Planet. Change* **162**, 18–27 (2018).
87. W. Knorr, A. Arneth, L. Jiang, Demographic controls of future global fire risk. *Nat. Clim. Chang.* **6**, 781–785 (2016).
88. F. Li, D. M. Lawrence, B. Bond-Lamberty, Impact of fire on global land surface air temperature and energy budget for the 20th century due to changes within ecosystems. *Environ. Res. Lett.* **12**, 044014 (2017).
89. G. Danabasoglu, NCAR CESM2 model output prepared for CMIP6 CMIP historical. Earth System Grid Federation. https://doi.org/10.22033/ESGF/CMIP6.7627. Accessed 20 March 2021.
90. J. P. Krasting *et al.*, NOAA-GFDL GFDL-ESM4 model output prepared for CMIP6 CMIP. Earth System Grid Federation. https://doi.org/10.22033/ESGF/CMIP6.1407. Accessed 20 March 2021.
91. R. Seferian, CNRM-CERFACS CNRM-ESM2-1 model output prepared for CMIP6 CMIP. Earth System Grid Federation. https://doi.org/10.22033/ESGF/CMIP6.1391. Accessed 20 March 2021.
92. L. M. Ulrike Groemping, Relative importance of regressors in linear models. (2021). https://cran.r-project.org/web/packages/relaimpo/relaimpo.pdf. Accessed 30 November 2021.
93. M. Z. Al-Hamdan *et al.*, Methods for characterizing fine particulate matter using ground observations and remotely sensed data: Potential use for environmental public health surveillance. *J. Air Waste Manag. Assoc.* **59**, 865–881 (2009).
94. H. Hersbach *et al.*, The ERA5 global reanalysis. *Q. J. R. Meteorol. Soc.* **146**, 1999–2049 (2020). https://www.ecmwf.int/en/forecasts/datasets/reanalysis-datasets/era5. Accessed 20 March 2021.
95. J. X. Wang, J. K. Angell, *Air Stagnation Climatology for the United States* (NOAA/Air Resource Laboratory ATLAS 1, Office of Oceanic and Atmospheric Research, Silver Spring, 1999).
96. S. Malyshev, E. Shevliakova, R. J. Stouffer, S. W. Pacala, Contrasting local versus regional effects of land-use-change-induced heterogeneity on historical climate: Analysis with the GFDL earth system model. *J. Clim.* **28**, 5448–5469 (2015).
97. E. Shevliakova *et al.*, Carbon cycling under 300 years of land use change: Importance of the secondary vegetation sink. *Global Biogeochem. Cycles* **23**, GB2022 (2009).
98. E. S. Weng *et al.*, Scaling from individual trees to forests in an Earth system modeling framework using a mathematically tractable model of height-structured competition. *Biogeosciences* **12**, 2655–2694 (2015).
99. K. Thonicke, S. Venevsky, S. Sitch, W. Cramer, The role of fire disturbance for global vegetation dynamics: Coupling fire into a dynamic global vegetation model. *Glob. Ecol. Biogeogr.* **10**, 661–677 (2001).
100. G. P. Compo *et al.*, The twentieth century reanalysis project. *Q. J. R. Meteorol. Soc.* **137**, 1–28 (2011).
101. D. M. Lawrence *et al.*, The Land Use Model Intercomparison Project (LUMIP) contribution to CMIP6: Rationale and experimental design. *Geosci. Model Dev.* **9**, 2973–2998 (2016).
102. V. Eyring *et al.*, Overview of the Coupled Model Intercomparison Project Phase 6 (CMIP6) experimental design and organization. *Geosci. Model Dev.* **9**, 1937–1958 (2016).
103. T. Hajima *et al.*, Development of the MIROC-ES2L Earth system model and the evaluation of biogeochemical processes and feedbacks. *Geosci. Model Dev.* **13**, 2197–2244 (2020).
104. L. W. Horowitz *et al.*, The GFDL global atmospheric chemistry-climate model AM4.1: Model description and simulation characteristics. *J. Adv. Model. Earth Syst.* **12**, e2019MS002032 (2020).
105. Ø. Seland *et al.*, Overview of the Norwegian Earth System Model (NorESM2) and key climate response of CMIP6 DECK, historical, and scenario simulations. *Geosci. Model Dev.* **13**, 6165–6200 (2020).
106. S. G. Coles, *An Introduction to Statistical Modeling of Extreme Values* (Springer Series in Statistics, Springer, New York, 2001).
107. H. E. Rieder, A. M. Fiore, L. W. Horowitz, V. Naik, Projecting policy-relevant metrics for high summertime ozone pollution events over the eastern United States due to climate and emission changes during the 21st century. *J. Geophys. Res. D Atmospheres* **120**, 784–800 (2015).
108. H. E. Rieder, A. M. Fiore, L. M. Polvani, J. F. Lamarque, Y. Fang, Changes in the frequency and return level of high ozone pollution events over the eastern United States following emission controls. *Environ. Res. Lett.* **8**, 014012 (2013).
109. L. Shen, L. J. Mickley, E. Gilleland, Impact of increasing heat waves on U.S. ozone episodes in the 2050s: Results from a multimodel analysis using extreme value theory. *Geophys. Res. Lett.* **43**, 4017–4025 (2016).
110. E. Gilleland, R. W. Katz, extRemes2.0: An extreme value analysis package in R. *J. Stat. Softw.* **72**, 1–39 (2016).